Improved Fusion of AIS Data for Multiple Extended Object Tracking

Martin Baerveldt[†], Jiangtao Shuai[‡] and Edmund Førland Brekke[†]

***Abstract*—In maritime situational awareness, the Automatic Identification System (AIS) is a vital source of information. Recent work has explored the fusion of AIS information and exteroceptive measurements to improve maritime target tracking performance, also for extended object tracking. However, in extended object tracking, the discrepancy between the center of the ship and the position reported by the AIS system is no longer negligible and is a source of systemic bias, which can degrade tracking performance. In this paper, we introduce a method for estimating this discrepancy based on AIS information and the estimation provided by the Gaussian process target model from the exteroceptive sensor data. We use this method combined with an extended object Poisson multi-Bernoulli mixture (PMBM) filter to perform multiple extended object tracking. We also introduce a specific method for initialization of targets using AIS measurements in this filter. We validate the proposed method with LiDAR and AIS data, collected from an inland waterway in Belgium. The results show that compensating for the bias in this manner results in better tracking performance, primarily due to better initialization of new targets.**

***Index Terms*—Automatic Identification System (AIS), Bayesian estimation, Extended targets, Data fusion, Multi-object tracking**

I. Introduction

Object tracking is an essential capability for a situational awareness system. It entails inferring information regarding objects of interest from noisy sensor data. Tracking multiple objects adds further complexity due to uncertainty in the association of measurements and number of objects [1]. Furthermore, if an object generates multiple measurements, extended object tracking methods can be used to estimate the shape and size, the extent, of the object in addition to its kinematic states. This provides more information, but necessitates more complex target models, further increasing the complexity of the problem [2]. To aid in tackling this complexity, one approach is to utilize information from target-provided measurements. In the field of waterborne transport, such target-provided data already exist in the form of the Automatic Identification System (AIS), a crucial system for vessel navigation. It allows the vessels to exchange information with other vessels and nearby shore stations, to increase the situational awareness of the crew, and help them avoid collisions with other vessels. This system is widespread and mandated by law for ships above a certain size (300 gross tonnage) and all passenger ships [3]. Therefore, it has a key role to play in tracking such ships [4]. AIS has also been used for collision avoidance systems for trials of an autonomous surface vehicle (ASV) [5]. The data provided by AIS can be fused with information from other sensors to perform multi-object tracking and recent studies have shown that this enhances tracking performance across various multi-object tracking frameworks [6]–[9]. Recent work has demonstrated how to incorporate target-provided measurements in multiple extended object tracking [10] using an extended object Poisson multi-Bernoulli mixture (PMBM) filter with a Gaussian process (GP) target model [11]. In this work, the AIS message is also used to estimate the size and shape of an object in addition to the kinematic states of position and velocity, which improved the extent estimation and tracking performance. However, fusing AIS information in the context of extended object tracking gives rise to additional challenges. One such challenge is the fact that in reality, the reported position in the AIS message does not necessarily correspond to the center of the ship. At sea, this minor discrepancy is not an issue, since the distances between vessels are generally quite large. However, when a ship is close enough for extended object tracking to be relevant, this discrepancy should be taken into account, especially for larger vessels. A specific environment where this is relevant is inland waterways, which are relatively narrow compared to the size of the vessels, meaning that vessels will pass close to one another. In this paper, we build on the work in [10] to develop a multiple extended object tracking method using AIS and LiDAR data and use it to track large (CEMT Class II or above [12]) vessels in an inland waterway, with data collected near the Albert Canal in Belgium. The main contributions compared to [10] include the estimation of the offset between the reported AIS position and the estimated centroid of the extended object, a more specific initialization procedure for AIS measurements, and the demonstration of the method in a dataset that combines LiDAR data with real AIS data. The paper is organized as follows; in Section II we present the relevant background theory, in Section III we present the specific method and our contributions and in Section IV we present the results on the gathered data, compared to the benchmark methods.

The research leading to these results has received funding from the European Union's Horizon 2020 research and innovation programme under the Marie Skłodowska-Curie grant agreement No 955.768 (MSCA-ETN AUTOBarge). This publication reflects only the authors' view, exempting the European Union from any liability. Project website: http://etn-autobarge.eu/. This work was supported in part by the Research Council of Norway through project 295033.

[†] Martin Baerveldt and Edmund Førland Brekke are with the Department of Engineering Cybernetics, NTNU, 7034 Trondheim, Norway
{martin.baerveldt, edmund.brekke}@ntnu.no

[‡] Jiangtao Shuai is with the Department of Mechanical Engineering, KU Leuven, B-3001 Leuven, Belgium
jiangtao.shuai@kuleuven.be

II. Background

In this section, we present the extent model used in this work, the GP model [13], then we give a summary of how the AIS data can be incorporated into this model and how it is combined in the PMBM framework, as described in [10].

A. Extended Object Tracking

Extended object tracking methods allow a given target to generate a varying number of measurements. This fact can be exploited to infer information about its shape and size from the spatial distribution of those measurements. An extended object tracking method requires a model for this spatial distribution. One common model is the random hypersurface model, which models the extent as a generic star-convex shape by parameterizing its contour [2]. This approach, in which the contour is modeled, naturally lends itself to representing contour-generated measurements, such as those obtained from LiDAR. To perform joint estimation of the extent and state of the target the following augmented state space vector can be defined

$$\mathbf{x}_k = \begin{bmatrix} \mathbf{x}_k^c & \phi_k & (\mathbf{x}_k^*) & \mathbf{x}_k^f \end{bmatrix}^\mathsf{T}, \tag{1}$$

where $\mathbf{x}_k^c$ is the position of the centroid of the target from which the extent is defined, ϕ_k is the heading of the target, and $\mathbf{x}_k^*$ are any additional kinematic states of the target. In our case, these are the velocity in each direction in 2D $\dot{\mathbf{x}}^c$, and the angular velocity $\dot{\phi}$. $\mathbf{x}_k^f$ is the parametrization of the contour of the extent. Using this state space vector, a generic measurement equation for this method can be written as

$$\begin{aligned} \mathbf{z}_k^l &= \mathbf{x}_k^c + \mathbf{p}(\theta_k^l) f(\theta_k^l) + \boldsymbol{\eta}_k^l \\ \mathbf{p}(\theta_k^l) &= \begin{bmatrix} \cos\theta_k^l \\ \sin\theta_k^l \end{bmatrix}. \end{aligned} \tag{2}$$

Where $\mathbf{z}_k^l$ is the measurement l at time k, θ_k^l is the corresponding angle of the origin of the measurement of the target contour and $f(\theta_k^l)$ is the radius function which parameterizes the extent. This radius function can be represented in a variety of ways, in this work, we use the GP method [13], for which a process model and a measurement model is defined. Furthermore, to handle the case when measurements are generated from the interior of the contour, a scaling factor can be used to model the distribution of the measurements over the surface. This was first presented in [14]. In the paper presenting the GP target model [13], this scaling factor was approximated as a Gaussian random variable according to

$$s_{k,l} \sim \mathcal{N}(\mu_s, \sigma_s^2). \tag{3}$$

For the specific case where the measurement source is uniformly distributed over the surface given by the star-convex shape, it was shown that $\mu_s = \frac{2}{3}$ and $\sigma_s^2 = \frac{1}{18}$. A measurement model for the GP target model applying this scaling factor was presented in [13]. Using this, we can define the measurement model used for the exteroceptive sensor measurements in this paper as follows.

$$\begin{aligned} \mathbf{z}_k^l &= \mathbf{h}_k^l(\mathbf{x}_k) + \boldsymbol{\eta}_k^l, \qquad \boldsymbol{\eta}_k^l \sim \mathcal{N}(0, \tilde{\mathbf{R}}_k^l) \\ \mathbf{h}_k^l(\mathbf{x}_k) &= \mathbf{x}_k^c + \mu_s \left(\mathbf{p}_k^l({\theta_k^l}^{(G)}(\mathbf{x}_k^c)) \mathbf{H}^f \left({\theta_k^l}^{(L)}(\mathbf{x}_k^c, \phi_k) \right) \mathbf{x}_k^f \right) \\ \tilde{\mathbf{R}}_k^l &= \mathbf{R}_k^l + \sigma_s^2 \tilde{\mathbf{H}}_k^l \mathbf{x}_k^f \left(\mathbf{x}_k^f \right)^\mathsf{T} \tilde{\mathbf{H}}_k^{l\mathsf{T}} \\ \tilde{\mathbf{H}}_k^l &= \mathbf{p}_k^l({\theta_k^l}^{(G)}(\mathbf{x}_k^c)) \mathbf{H}^f \left({\theta_k^l}^{(L)}(\mathbf{x}_k^c, \phi_k) \right) \\ \mathbf{R}_k^l &= \mathbf{p}_k^l(\mathbf{x}_k^c) \mathbf{R}^f \left({\theta_k^l}^{(L)}(\mathbf{x}_k^c, \phi_k) \right) \mathbf{p}_k^l(\mathbf{x}_k^c)^\mathsf{T} + \mathbf{R}. \end{aligned} \tag{4}$$

Here $\mathbf{R}$ is the inherent measurement noise of the exteroceptive sensor, θ_k^l is defined either in the global frame ${\theta_k^l}^{(G)}$ or the local target frame ${\theta_k^l}^{(L)}$ as

$$\begin{aligned} {\theta_k^l}^{(L)}(\mathbf{x}_k^c, \phi_k) &= {\theta_k^l}^{(G)}(\mathbf{x}_k^c) - \phi_k \\ {\theta_k^l}^{(G)}(\mathbf{x}_k^c) &= \angle \left(\mathbf{z}_{k,l} - \mathbf{x}_k^c \right) \end{aligned} \tag{5}$$

and $\mathbf{H}^f$ and $\mathbf{R}^f$ are found by Gaussian process regression, which in turn is defined by a specific covariance function. The covariance function can be defined to encode axial symmetry, for instance, along the longitudinal axis. For more details and exact expressions, see [11]. This measurement model is non-linear and therefore an extended Kalman filter is used to perform the state estimation. Furthermore, iterations can be added to improve the linearization which turns the problem into a Gauss-Newton optimization problem, which allows additional criteria to be defined which avoids convergence to local optima [11].

B. AIS Data in Extended Object Tracking

The AIS protocol defines different message types for carrying different types of information. Kinematic data, i.e., position, course over ground, speed, and heading, are reported in a position report that is regularly broadcast by all ships with AIS transmitters (message type 1). The period between transmission is at most 10 s for vessels moving under their own power [15, Annex 1]. We can define a measurement equation for the contents of this message as

$$\begin{aligned} \mathbf{p}^{AIS} &= \mathbf{x}^c + \boldsymbol{\eta}_{\boldsymbol{p}} & \boldsymbol{\eta}_{\boldsymbol{p}}, &\sim \mathcal{N}(0, \sigma_p^2 \mathbf{I}_2) \\ |\mathbf{v}^{AIS}| R\left(\angle \mathbf{v}^{AIS}\right) &= \dot{\mathbf{x}}^c + \boldsymbol{\eta}_{\boldsymbol{v}} & \boldsymbol{\eta}_{\boldsymbol{v}}, &\sim \mathcal{N}(0, \mathbf{R}_v) \\ \psi^{AIS} &= \phi + \boldsymbol{\eta}_{\boldsymbol{\psi}}, & \boldsymbol{\eta}_{\boldsymbol{\psi}} &\sim \mathcal{N}(0, \sigma_\psi^2) \end{aligned} \tag{6}$$

where $\mathbf{p}^{AIS}$ is the reported position with corresponding measurement noise standard deviation σ_p. $|\mathbf{v}^{AIS}|$ is the reported speed, $\angle \mathbf{v}^{AIS}$ is the reported course and $\mathbf{R}_v$ is a Cartesian conversion of the polar measurement noise matrix given by the angular and radial standard deviation $\sigma_{\angle v}$ and $\sigma_{|v|}$ respectively. ψ^{AIS} is the reported heading with the corresponding measurement noise standard deviation σ_ψ. Ship dimensions are instead reported in a different message containing static ship and voyage-related data (message type 5) [15, Annex 8]. The data contained in this message is self-reported, i.e., it has to be filled in manually by the ship's crew and it also has to be updated if any information changes. To define a measurement

model for the dimensions, we note that the length and width of the ship are related to the radius function $f(\theta)$ at specific fixed angles corresponding to the length and width [10].

$$\begin{aligned} L^{AIS} &= f(0) + f(\pi) \\ W^{AIS} &= f(\pi/2) + f(3\pi/2). \end{aligned} \tag{7}$$

Utilizing the GP target model, this expression can be written as

$$\begin{aligned} L^{AIS} &= \left(\mathbf{H}^f(0) + \mathbf{H}^f(\pi)\right)\mathbf{x}^f + \mathbf{w}^L \\ W^{AIS} &= \left(\mathbf{H}^f\left(\frac{\pi}{2}\right) + \mathbf{H}^f\left(\frac{3\pi}{2}\right)\right)\mathbf{x}^f + \mathbf{w}^W \\ \mathbf{w}^L &\sim \mathcal{N}(0, \mathbf{R}^L), \qquad \mathbf{w}^W \sim \mathcal{N}(0, \mathbf{R}^W). \end{aligned} \tag{8}$$

The estimated measurement noise also has a component for GP regression, which is given by

$$\begin{aligned} \mathbf{R}^L &= \mathbf{R}^f(0) + \mathbf{R}^f(\pi) + \sigma_{\mathbf{d}}^2 \\ \mathbf{R}^W &= \mathbf{R}^f\left(\frac{\pi}{2}\right) + \mathbf{R}^f\left(\frac{3\pi}{2}\right) + \sigma_{\mathbf{d}}^2, \end{aligned} \tag{9}$$

where $\sigma_{\mathbf{d}}$ is the measurement noise for the dimensions reported by the AIS message. The combined measurement model matrix for an AIS measurement can be written as

$$\begin{aligned} \mathbf{H}^{AIS} &= \begin{bmatrix} \mathbf{H}^{kin} & \mathbf{0} \\ \mathbf{0} & \mathbf{H}_d \end{bmatrix} \\ \mathbf{H}^{kin} &= \mathrm{diag}[1,1,1,1,1] \\ \mathbf{H}^{d} &= \begin{bmatrix} \mathbf{H}^f(0) + \mathbf{H}^f(\pi) \\ \mathbf{H}^f\left(\frac{\pi}{2}\right) + \mathbf{H}^f\left(\frac{3\pi}{2}\right) \end{bmatrix}. \end{aligned} \tag{10}$$

The combined measurement noise matrix $\mathbf{R}^{AIS}$ can be constructed by combining the different measurement noise matrices in a block diagonal fashion.

C. AIS Data in the PMBM Filter

The PMBM filter is a multi-object filter that utilizes a Poisson point process (PPP) to model undetected targets and a multi-Bernoulli mixture (MBM) to model detected targets. A PMBM density is fully parametrized by the following parameters

$$D_k^u, \{w_k^j, \{r_k^{j,i}, (f_k^{j,i})\}_{i\in\mathbb{I}_{k|k'}}\}_{j\in\mathbb{J}_{k|k'}}. \tag{11}$$

Where D_k^u is the intensity function of the PPP for the unknown targets. The Bernoulli modeling target i is represented by the probability density $f_k^{j,i}$, and a parameter r that represents the existence probability of the target. The components in the multi-Bernoulli mixture are represented by an index $j \in \mathbb{J}$ and correspond to a data association hypothesis with the weight w^j representing the relative likelihood of each hypothesis. For an extended object, each target is detected with a probability P^D and if detected, generates measurements according to a PPP with rate $\lambda_m(\mathbf{x})$ and a spatial distribution $l(Z_C|\mathbf{x}_k)$. Z_C is the subset of measurements assigned to a specific measurement cell C, and l_C is the likelihood of this assignment. Clutter is modelled as a PPP with rate λ_c. Recursions based on these assumptions are presented in the original paper on the PMBM filter for extended objects [16] and adapted for a GP target model in [11]. For the GP model, a single object estimate is represented by gamma-Gaussian distributions according to

$$f = \mathcal{N}(\mathbf{x}; \hat{\mathbf{x}}, \mathbf{P})\mathcal{G}(\alpha, \beta). \tag{12}$$

The Gaussian component is given by the state space vector defined in the section above, whereas the gamma distribution provides an estimate of $\lambda_m(\mathbf{x})$ governing the cardinality of the measurement set associated with a target. Recursions are defined according to

$$\begin{aligned} \alpha_{k|k-1} &= \frac{\alpha_{k-1}}{\eta_\gamma}, \qquad \beta_{k|k-1} = \frac{\beta_{k-1}}{\eta_\gamma} \\ \alpha_k &= \alpha_{k|k-1} + |Z_C|, \qquad \beta_k = \beta_{k|k-1} + 1, \end{aligned} \tag{13}$$

where η_γ is defined as $\eta_\gamma = \frac{1}{1-\frac{1}{w_e}}$, which means that only information from the time steps within the window length w_e is trusted [17].

We omit the full recursions for the PMBM filter using the GP target model and refer to [11] or [10] for these. We instead highlight the part of the recursions that are affected by the different kinds of measurements. Of the above quantities, the likelihood of a measurement assignment l_C and the calculation of the individual posterior densities represented by $f_k^{j,i}$ are affected by the choice of measurement model, and thus whether it is an exteroceptive measurement or a target-provided measurement. For exteroceptive measurements l_C is given by

$$l_C = P_D \frac{\Gamma(\alpha + |Z_C|)\beta^\alpha}{\Gamma(\alpha)(\beta+1)^{(\alpha+|Z_C|)}|Z_C|!} \times \prod_{z\in Z_C} \mathcal{N}(z^l; \bar{\mathbf{z}}^l, \mathbf{S}^l), \tag{14}$$

where $\bar{\mathbf{z}}^l$ and $\mathbf{S}^l$ are given by the measurement model in (4). The posterior densities are given by a Kalman filter update step using the same measurement model for the Gaussian component and by (13) for the gamma component. For target-provided measurements, l_C is given by

$$l_C = p_\tau(\tau^{\mathbf{z}}|\tau)\mathcal{N}(\mathbf{z}^{AIS}; \bar{\mathbf{z}}^{AIS}, \mathbf{S}^{AIS}), \tag{15}$$

where $\bar{\mathbf{z}}^{AIS}$ and $\mathbf{S}^{AIS}$ are given by the measurement model in (10) and $p_\tau(\tau^{\mathbf{z}}|\tau)$ is the likelihood of the AIS measurement ID $\tau^{\mathbf{z}}$ being the same as the target ID τ, which is given by

$$p_\tau(\tau^{\mathbf{z}}|\tau) = \begin{cases} P_C & \text{if} \quad \tau = \tau^{\mathbf{z}} \\ \frac{1-P_C}{|\mathcal{V}|-1} & \text{if} \quad \tau \neq \tau^{\mathbf{z}} \\ 0 & \text{if} \quad \tau = 0 \end{cases}, \tag{16}$$

where P_C is the probability of a correct ID and $|\mathcal{V}|$ is the total number of possible IDs. Furthermore, P_D and the clutter rate λ_c are modified for target-provided measurements, they are defined to have no impact on the likelihoods by defining

$$\begin{aligned} P_D &= \begin{cases} 1 & \text{if a measurement is received} \\ 0 & \text{Otherwise} \end{cases} \\ \lambda_c &= 0. \end{aligned} \tag{17}$$

For more details on the combination of target-provided and exteroceptive measurements for extended objects in the PMBM framework, see [10].

III. Method

In this section, we present how we estimate the discrepancy between the reported AIS position and the estimated centroid as well as how targets are initialized using AIS measurements.

A. Bias Estimate

Recall that the dimensions of a vessel are reported in a specific AIS message type. The actual structure of this message also contains information about the location of the reference point for the reported position on the ship [15, Annex 8]. This is done by reporting four values where A is the distance from the bow to the reference point, B is the distance from the stern, C is the distance from the port side and D is the distance from the starboard side, this means that the length is given by $A + B = L^{AIS}$ and the width $C + D = W^{AIS}$. However, the reference point of the position is not always available since it is not required for all vessels, and this is indicated by $A = C = 0$. This information can be redefined to a longitudinal and lateral distance in a local target frame according to

$$\delta x = \frac{A+B}{2} - A, \qquad \delta y = \frac{C+D}{2} - C, \tag{18}$$

where δx is the longitudinal and δy is the lateral offset from the center of the ship. A graphical representation of these variables can be seen in Fig. 1. With a known offset, we can define a refined expression for the reported AIS position as

$$\mathbf{p}^{AIS} = \mathbf{x}^c + R(\phi) \begin{bmatrix} \delta x \\ \delta y \end{bmatrix}, \tag{19}$$

where $R(\phi)$ is the 2D rotational matrix. The simplest choice would therefore be to use this expression directly and assume that the information is correct. However, this relies on the provided information being reported correctly, if it is provided at all. Therefore, there is a potential for errors. The other issue is the fact that the centroid $\mathbf{x}^c$ is directly affected, which could affect the estimate of the extent. Therefore, we propose an alternative approach where we estimate δx and δy as unknown quantities and as part of the state vector. This can be seen as a form of bias estimation. Therefore, the new measurement equation for the reported AIS position is given by (19), and the Jacobian of this expression is used in the measurement model matrix $\mathbf{H}^{AIS}$ for the AIS update step.

The process model for these offset terms can be defined from the Wiener process, which is a common process model for unknown time-varying biases [18], which defines the process model matrices as follows

$$\mathbf{F}^{\delta} = \mathbf{I}, \qquad \mathbf{Q}^{\delta} = \sigma_{\delta}^2 T \mathbf{I}, \tag{20}$$

where σ_δ is the variance and T is the sampling time. These matrices are then used as an augmentation of the process model of the target model. The practical effect of this is that as the AIS measurements arrive, the centroid of the ship that is used to define the extent will be estimated using the exteroceptive sensor measurements and the estimated offset will be estimated by the difference between the reported AIS position and the estimated centroid. Therefore, it should be expected to converge after a few AIS measurements have been received. If the reference point of the reported position is available via AIS, this should also be used, in this work we use it as a prior to initialize the estimate, which should allow the bias to converge faster. We should also note that by estimating this bias, we could potentially capture other sources of systemic biases. One such source could be errors in time synchronization between the AIS and exteroceptive sensor measurements.

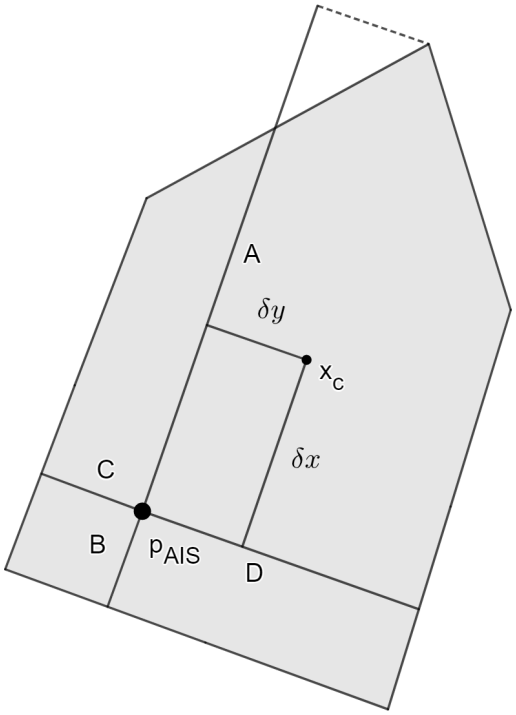

Fig. 1. A visualization of the definition of the AIS message content A, B, C, and D, along with the definition of δx and δy

B. Initialization for Multi-Object Tracking

The multi-object tracking method is similar to the one presented in [10]. However, in this work, we want to study in more detail the case where AIS measurements are received before the exteroceptive measurements, which will be the case in reality. Therefore, the AIS measurement will be used to initialize a track, which is preferable since it provides more information. It should be noted that while the heading can be reported via AIS, no ship that we observed during data gathering reported this information, and thus we can assume that it is fairly rare. However, the course is always reported and for initialization, we suggest that it be used as a measurement for the heading. If the antenna offset is available from the AIS message, we augment the AIS measurement with a direct measurement of δx and δy, this will provide an initial guess of the value which can be refined when

exteroceptive measurements are received. Therefore, we define an augmentation of (6), which is used when initializing a target

$$\begin{aligned} \angle \mathbf{v}^{AIS} &= \phi + \boldsymbol{\eta}_{\angle \mathbf{v}}, & \boldsymbol{\eta}_{\angle \mathbf{v}} &\sim \mathcal{N}(0, \sigma^2_{\angle \mathbf{v}}) \\ \delta x^{AIS} &= \delta x + \boldsymbol{\eta}_{\boldsymbol{\delta 0}}, & \boldsymbol{\eta}_{\boldsymbol{\delta 0}} &\sim \mathcal{N}(0, \sigma^2_d) \\ \delta y^{AIS} &= \delta y + \boldsymbol{\eta}_{\boldsymbol{\delta 0}}, & \boldsymbol{\eta}_{\boldsymbol{\delta 0}} &\sim \mathcal{N}(0, \sigma^2_d). \end{aligned} \tag{21}$$

We also use the AIS-reported width and length to explicitly define the extent of the newly born target. We only do this if a new target is detected by an AIS measurement, i.e., for AIS measurements associated with the PPP component. However, this is only used for the calculation of the posterior density, and not for the calculation of l_C since the relative likelihood of this augmented measurement would not be directly comparable with hypotheses where the AIS measurement is associated with a Bernoulli component.

Related to this, we will often have cases where an AIS measurement initializes a target beyond the range of the exteroceptive sensor. If this happens, subsequent updates using exteroceptive sensor measurements will lower the existence probability of the target since it will be counted as a misdetection until the target is in range of the sensor. To mitigate this, we can redefine the probability of detection P_D based on the distance of an object to the sensor. However, we need to consider that a measurement is generated along the contour and that an object is in range of a sensor when a part of the contour is in range, so we need to calculate the distance to the closest point. To do this, we calculate the distance to each sampling point on the extent and then take the closest distance, i.e.,

$$d_{obj}(\mathbf{x}) = \min(||\mathbf{x}^c + R(\phi + \Theta^f)\mathbf{x}^f||). \tag{22}$$

Here, Θ^f is the vector of test angles, the angles at which the radius of the contour is given by the contents of the vector $\mathbf{x}^f$. This allows us to calculate a range dependent value of P_D for each component of the PMBM which we do according to

$$P_D(\mathbf{x}) = \begin{cases} P_D & d_{obj} < R_{ex} \\ P_D(1 - \frac{d_{obj}(\mathbf{x}) - R_{ex}}{\delta R_{ex}}) & 0 < d_{obj} - R_{ex} < \delta R_{ex} \\ 0 & \text{otherwise} \end{cases}. \tag{23}$$

Here R_{ex} is the stated range of the exteroceptive sensor and we use the linearily descending function defined by δR_{ex} to handle eventual returns beyond that. The gamma parameters will also decrease once a target has been detected due to the prediction step in the recursions defined by (13). Therefore, the parameter that governs this prediction should be set to $\eta_\gamma = 1$ before the exteroceptive sensor detects the target to prevent the expected number of measurements from decreasing.

IV. Experimental Data

In this section, we present results where LiDAR and AIS data was gathered using the sensor box described in [19], which is an upgraded version of [20]. We compare three different PMBM filters using the GP target model, one where we do not utilize any AIS information, corresponding to [11], denoted GP, one where we do not consider the offset in the AIS estimate, corresponding to [10], denoted GP+AIS, and the proposed method, denoted GP+AIS+bias.

A. Methodology

The data was gathered by placing the sensor box on the shore of the Albert Canal, a large inland waterway in Belgium, and scanning the ships that passed by. The mechanical LiDAR had a maximum detection range of 150 m (which means that R_{ex} = 150 m, and δR_{ex} = 25 m) and it was spinning at a frequency of 10 Hz. AIS data was gathered with an external AIS receiver. Land returns were removed as part of manual post-processing. To obtain ground truth data, the data was labeled manually by inspecting the LiDAR scans to identify the extent of the ships, the AIS data for speed and course was interpolated to attain the velocity, and the course was also used as a proxy for the heading. This allows us to reconstruct the shape of the hull so that it can be used to get a measure of the quality of the extent estimate. From the data set, we select two scenarios for further study. One is a scenario with a single ship, and the other is two ships meeting each other in front of the sensor.

B. Metrics

We use the same metrics as in [11], that is, intersection-over-union and heading error to compare the extent estimation and the GOSPA metric, which aggregates localization error, the number of missing targets, and the number of false targets into one metric, to compare multi-object tracking performance [21]. The state variables used in the GOSPA metric are the position variables for the centroid, an estimate is reported if its probability of existence is higher than 0.5, and parameters for the GOSPA metric were cut off $c = 40$ and power $p = 2$.

C. Parameters

The parameters are defined as follows, we use σ_c = 0.01 $\sqrt{m^2 s^{-3}}$ as the noise parameter for the constant velocity model, σ_ϕ = 0.0001 $\sqrt{rad^2 s^{-3}}$ as noise for the constant angular velocity model, and σ_r = 0.1 m for the measurement noise. We use 20 for the length of the gamma prediction window. We use 16 test angles to parametrize the extent and the hyperparameters are σ_f = 1 m, σ_r = 4 m, σ_n = 0.01 m, $l = \pi/6$ rad and the forgetting factor $\eta_f = 0.005$. The maximum amount of IEKF iterations is 50. For the AIS measurement noise, we use $\sigma_p = 1$ m, $\sigma_{\angle v} = 0.001$ rad, $\sigma_{|v|} = 0.1$ m/s, $\sigma_\phi = 0.001$ rad and $\sigma_d = 0.5$ m. The process noise for the offset estimate is $\sigma_\delta = 0.001$ m. The birth density is defined with two components at a distance of 200 m from the sensor at either side of the canal, where the prior heading and course angle are aligned with the direction of the canal. The prior speed is assumed to be $v_0 = 3$ m/s and the extent prior is defined as a rectangle 60 m long and 10 m wide, with a pointed bow at the front which is 6 m deep. The prior value of the gamma distribution is $\alpha_0 = 1000$ and $\beta_0 = 100$. The initial covariance is defined with the following standard deviations, the positional components are 30 m, the velocity components are 0.1 m/s, the heading component is $\pi/4$ rad

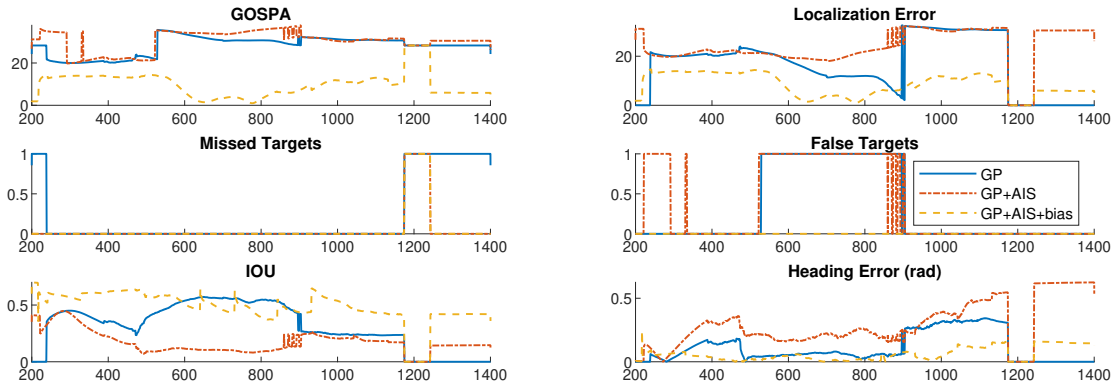

Fig. 2. Evolution over time for the three methods for selected metrics for a single ship

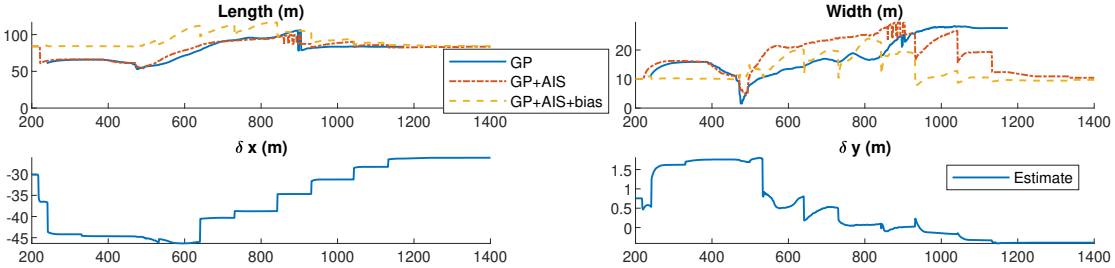

Fig. 3. Evolution over time of the estimates of the dimensions of the ship, as well as the estimate of the bias provided by our proposed method

TABLE I
MEAN VALUE FOR THE METRICS FOR THE FIRST SCENARIO

Method	GP	GP+AIS	GP+AIS+bias
GOSPA	28.20	30.49	**9.98**
Loc. Err.	20.94	24.99	**8.88**
Missed	0.19	0.05	**0.05**
False	0.26	0.31	**0.00**
IOU	0.40	0.18	**0.51**
Heading (rad)	0.14	0.31	**0.06**

and the angular velocity is $\pi/20$ rad/s. The offset estimates have an initial standard deviation of 30 and 5 m for δx and δy respectively. The PMBM parameters are chosen as follows, probability of detection $P_D = 0.90$, probability of survival $P_S = 0.999$, and clutter rate $\lambda_c = 20$. The gating probability is set at $P_G = 0.99$, the pruning parameters are 0.01 for the existence probability, 0.001 for PPP mixture components, and 0.01 for multi-Bernoulli mixture components.

D. Single Target

The mean values of the metrics are presented in Table I. The evolution of the metrics over time is shown in Fig. 2. Here, we note that most of the benefit of our proposed method comes from the initial stages, with no false targets and a better state estimate. Our method initializes the track earlier and with the correct dimensions. However, when not compensating for the offset, the discrepancy between the LiDAR and AIS measurements results in large errors in the extent estimation due to large heading errors. When the LiDAR detects the rear of the ship, these measurements are associated as belonging to a new target, resulting in a false target, which in turn is not associated with the AIS measurements. This also contributes to a poor extent estimate and shows that accounting for the antenna offset is essential when combining exteroceptive and AIS measurements in a multiple extended object tracking framework. LiDAR measurements cease coming from the vessel around timestep 1200, resulting in the target being missed for those timesteps, but when the next AIS measurement arrives the ship continues to be tracked, note that the tracking performance is better when the offset has been estimated.

We can also study how well the methods estimate the length and width. This is presented in Fig. 3. Note the see-saw pattern for both the length and width estimates when AIS measurements arrive, which matches with a similar pattern in the IOU metric. This indicates that the extent model overestimates both length and width. A significant reason for this is the choice of the scaling factor s, since the measurements are assumed to be uniformly distributed across the extent surface. For a LiDAR, this is not accurate and if the measurements originate more from the contour, the extent will be overestimated. We can observe this effect in Fig. 4 by the fact that the measurements are enclosed by the estimate, showing the conservative nature of the use of a scaling factor, particularly with fewer measurements. Using AIS measurements mitigates this since exact dimensions are measured, giving indents in the estimates on

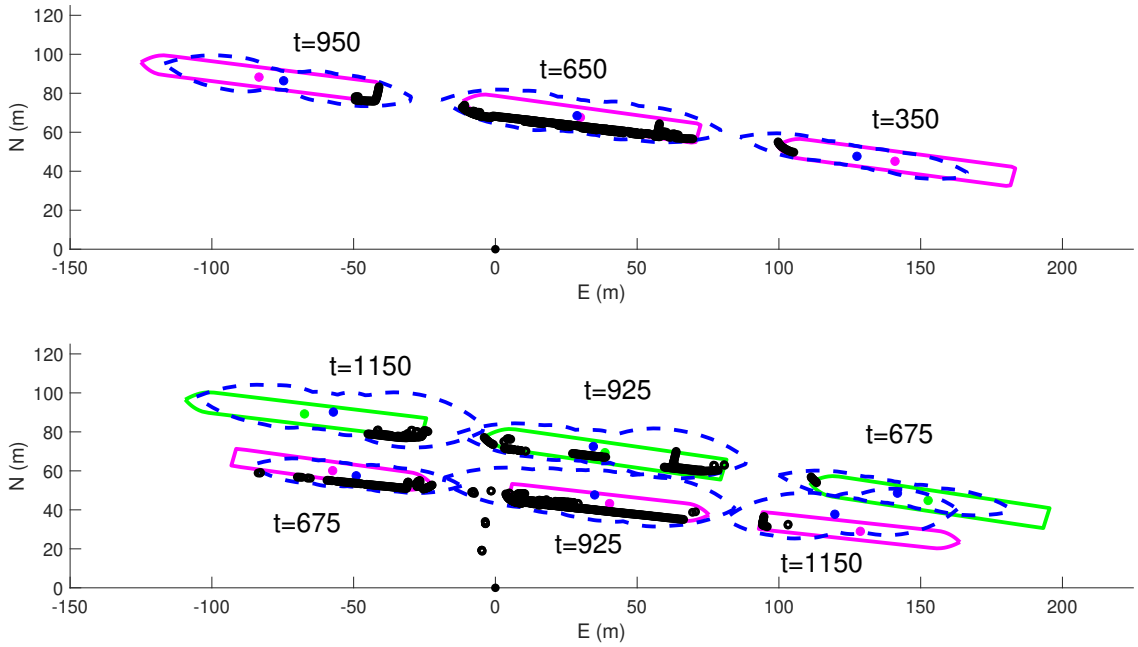

Fig. 4. Three different representative timesteps visualized for both scenarios with the single target scenario above and the multiple targets below. The ground truth is shown as the magenta solid line, with the centroid as a dot, or green for the other ship in the multiple target scenario. The estimated extent of our proposed method is shown as the dashed blue line with a blue dot representing the centroid, along with LiDAR measurements represented by black circles.

either side of the estimated centroid, keeping it smaller than it otherwise would have been. The width suffers from not only the scaling factor issue but also the issue of modeling very elongated shapes using a radial function. The reason for the use of a scaling factor despite these drawbacks is that it allows the full point cloud to be used for the state estimation. It also resulted in much more stable estimates when compared to the regular contour model, even when measurements from within the contour were removed.

Regarding the bias, it can be seen to converge quickly, after receiving a second AIS measurement. However, it does not converge to a constant value, particularly after timestep 600 when the ship passes the sensor. This is due to the estimated position of the centroid moving due to the influence of the target model, which can be seen in Fig. 4. The main contributor is the choice of the scale factor, which causes the centroid to be initialized in front of the actual center of the ship. It then moves rearward when compared to the ground truth, ending up behind it at the end of the run. Therefore, the centroid of the estimate does not necessarily correspond to the geometric centroid of the object, especially if only a part of the object is visible. Regardless of this variation, this shows that the bias can be estimated using this technique, but since the centroid can move, it might not converge to a fixed value.

E. Multiple Targets

The scenario itself can be seen in Fig. 4. Note that the furthermost vessel from the sensor is not fully occluded during the scenario due to the usage of the full 3D point cloud. The mean values of all the metrics are presented in Table II and the evolution of the metrics over time is shown in Fig. 5. The results follow a similar trend as for the single targets, and again we can note the improved initialization of targets for the proposed method and the resulting lack of missed and false targets compared to the other methods, which both produce an additional estimate for the furthermost vessel from the sensor. We can also note the impact of clutter from the wake in the shape of the estimate in Fig. 4 at t = 925, which elongates the estimate behind the ship.

TABLE II
MEAN VALUE FOR THE METRICS FOR THE SECOND SCENARIO

Method	GP	GP+AIS	GP+AIS+bias
GOSPA	37.71	40.86	**16.34**
Loc. Err.	23.75	44.39	**17.19**
Missed	0.33	0.11	**0.08**
False	0.35	0.22	**0.00**
IOU	0.33	0.28	**0.44**
Heading (rad)	0.13	0.38	**0.08**

V. CONCLUSION

In this work, we have presented a method that utilizes AIS and LiDAR data to perform multiple extended object tracking on larger (CEMT Class II or above [12]) vessels found in inland waterways. In particular, we have shown how to utilize both measurement sources to estimate the bias between the reported AIS position and the estimated centroid of an

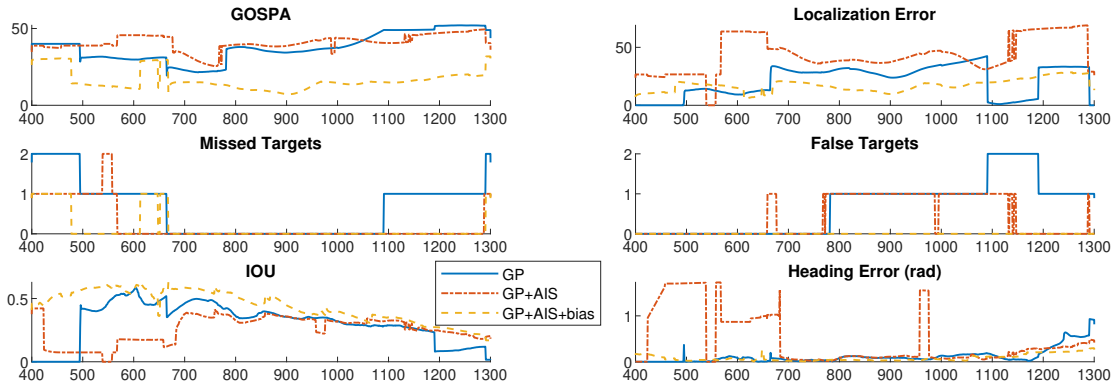

Fig. 5. Evolution over time for the three methods for selected metrics for multiple ships

extended object, along with how to handle the specific case when a target is initialized with an AIS measurement. We have also demonstrated this method on real data, finding a particular benefit for the proposed method in the initialization of targets. It should be noted that while LiDAR was used as the sensor in this work, in principle, it should work with any exteroceptive sensor. Future work could focus on improving the extent model to be able to more accurately represent ship shapes, along with finding a better choice of scale parameter, or a different manner of handling measurements from within the contour. It could also be of interest to incorporate smoothing in this method, since this could remove the see-saw patterns of corrections when new AIS measurements arrive and distribute the accumulated error, improving the estimate.

REFERENCES

[1] B. Vo, M. Mallick, Y. Bar-Shalom, S. Coraluppi, R. Osborne, R. Mahler, and B. Vo, "Multitarget Tracking," 2015. [Online]. Available: https://onlinelibrary.wiley.com/doi/10.1002/047134608X.W8275

[2] K. Granström, M. Baum, and S. Reuter, "Extended Object Tracking: Introduction, Overview and Applications," *Journal of Advances in Information Fusion*, vol. 12, no. 2, pp. 139–174, Dec. 2017.

[3] International Maritime Organization (IMO), "AIS Transponders," 2019, accessed 11-March-2024. [Online]. Available: https://www.imo.org/en/OurWork/Safety/Pages/AIS.aspx

[4] S. Thombre, Z. Zhao, H. Ramm-Schmidt, J. M. Vallet García, T. Malkamäki, S. Nikolskiy, T. Hammarberg, H. Nuortie, M. Z. H. Bhuiyan, S. Särkkä, and V. V. Lehtola, "Sensors and AI Techniques for Situational Awareness in Autonomous Ships: A Review," *IEEE Transactions on Intelligent Transportation Systems*, vol. 23, no. 1, pp. 64–83, Jan. 2022.

[5] D. K. M. Kufoalor, T. A. Johansen, E. F. Brekke, A. Hepsø, and K. Trnka, "Autonomous maritime collision avoidance: Field verification of autonomous surface vehicle behavior in challenging scenarios," *Journal of Field Robotics*, vol. 37, no. 3, pp. 387–403, 2020.

[6] A. G. Hem and E. F. Brekke, "Variations of Joint Integrated Data Association With Radar and Target-Provided Measurements," *Journal of Advances in Information Fusion*, vol. 17, no. 2, pp. 97–115, Dec. 2022.

[7] B. Habtemariam, R. Tharmarasa, M. McDonald, and T. Kirubarajan, "Measurement level AIS/radar fusion," *Signal Processing*, vol. 106, pp. 348–357, Jan. 2015.

[8] T. Miao, E. E. Amam, P. Slaets, and D. Pissoort, "Multi-Target Tracking and Detection, fusing RADAR and AIS Signals using Poisson Multi-Bernoulli Mixture Tracking, in support of Autonomous Sailing," in *Proceedings of the International Naval Engineering Conference & Exhibition (INEC)*, Oct. 2020.

[9] D. Gaglione, P. Braca, G. Soldi, F. Meyer, F. Hlawatsch, and M. Z. Win, "Fusion of Sensor Measurements and Target-Provided Information in Multitarget Tracking," *IEEE Transactions on Signal Processing*, vol. 70, pp. 322–336, 2022.

[10] A. G. Hem, M. Baerveldt, and E. F. Brekke, "PMBM filtering with fusion of target-provided and exteroceptive measurements: Applications to maritime point and extended object tracking," *IEEE Access*, vol. 12, pp. 55 404–55 423, 2024.

[11] M. Baerveldt, M. E. Lopez, and E. F. Brekke, "Extended target PMBM tracker with a Gaussian Process target model on LiDAR data," in *2023 26th International Conference on Information Fusion (FUSION)*, Jun. 2023.

[12] Wikipedia contributors, "Classification of european inland waterways — Wikipedia, the free encyclopedia," 2024, accessed 7-March-2024. [Online]. Available: https://en.wikipedia.org/w/index.php?title=Classification_of_European_Inland_Waterways&oldid=1211382457

[13] N. Wahlström and E. Özkan, "Extended Target Tracking Using Gaussian Processes," *IEEE Trans. Signal Process.*, vol. 63, no. 16, pp. 4165–4178, Aug. 2015.

[14] M. Baum and U. D. Hanebeck, "Shape tracking of extended objects and group targets with star-convex RHMs," in *2011 14th International Conference on Information Fusion (FUSION)*, Jul. 2011.

[15] ITU-R, "M.1371: Technical characteristics for an automatic identification system using time division multiple access in the VHF maritime mobile frequency band." [Online]. Available: https://www.itu.int/rec/R-REC-M.1371-5-201402-I/en

[16] K. Granström, M. Fatemi, and L. Svensson, "Poisson Multi-Bernoulli Mixture Conjugate Prior for Multiple Extended Target Filtering," *IEEE Transactions on Aerospace and Electronic Systems*, vol. 56, no. 1, pp. 208–225, Feb. 2020.

[17] K. Granström and U. Orguner, "Estimation and maintenance of measurement rates for multiple extended target tracking," in *2012 15th International Conference on Information Fusion (FUSION)*, Jul. 2012, pp. 2170–2176.

[18] Y. Bar-Shalom, X. Li, and T. Kirubarajan, *Estimation with Applications to Tracking and Navigation: Theory, Algorithms and Software*. John Wiley & Sons, 01 2004.

[19] J. Shuai, S. Van Baelen, J. Billet, T. Schamp, Y.-Y. Zhang, and P. Slaets, "A multimodal sensor box for inland waterways: Design, build, and experiment," *Presented at the International Conference on Maritime Autonomous Surface Ship (ICMASS)*, Nov. 2023.

[20] S. Van Baelen, J. Shuai, R. Amsters, T. Schamp, and P. Slaets, "Situational awareness on inland waterways with multimodal, standalone sensor box: design and experiments," in *OCEANS 2023 - Limerick*, Jun. 2023.

[21] A. S. Rahmathullah, A. F. García-Fernández, and L. Svensson, "Generalized optimal sub-pattern assignment metric," in *2017 20th International Conference on Information Fusion (FUSION)*, Jul. 2017.